Measurements of branching fractions of $\Lambda_c^+ \to \Sigma^+\eta$ and $\Lambda_c^+ \to \Sigma^+\eta'$ and asymmetry parameters of $\Lambda_c^+ \to \Sigma^+\pi^0$, $\Lambda_c^+ \to \Sigma^+\eta$, and $\Lambda_c^+ \to \Sigma^+\eta'$

S. X. Li, C. P. Shen, I. Adachi, J. K. Ahn, H. Aihara, D. M. Asner, H. Atmacan, T. Aushev, R. Ayad, V. Babu, S. Bahinipati, Sw. Banerjee, P. Behera, K. Belous, J. Bennett, M. Bessner, T. Bilka, D. Biswas, A. Bobrov, D. Bodrov, J. Borah, M. Bračko, P. Branchini, T. E. Browder, A. Budano, M. Campajola, D. Červenkov, M.-C. Chang, P. Chang, V. Chekelian, A. Chen, B. G. Cheon, K. Chilikin, H. E. Cho, K. Cho, S.-J. Cho, S.-K. Choi, Y. Choi, S. Choudhury, D. Cinabro, G. De Pietro, R. Dhamija, F. Di Capua, T. V. Dong, T. Ferber, A. Frey, B. G. Fulsom, V. Gaur, A. Giri, P. Goldenzweig, E. Graziani, T. Gu, K. Gudkova, C. Hadjivasiliou, K. Hayasaka, H. Hayashii, C.-L. Hsu, K. Inami, N. Ipsita, A. Ishikawa, R. Itoh, W. W. Jacobs, Y. Jin, K. K. Joo, D. Kalita, A. B. Kaliyar, C. Kiesling, C. H. Kim, D. Y. Kim, K.-H. Kim, Y.-K. Kim, P. Kodyš, T. Konno, A. Korobov, S. Korpar, E. Kovalenko, P. Krokovny, T. Kuhr, M. Kumar, R. Kumar, K. Kumara, A. Kuzmin, Y.-J. Kwon, T. Lam, J. S. Lange, S. C. Lee, L. K. Li, Y. Li, Y. B. Li, L. Li Gioi, J. Libby, K. Lieret, M. Masuda, T. Matsuda, S. K. Maurya, F. Meier, M. Merola, F. Metzner, R. Mizuk, R. Mussa, I. Nakamura, M. Nakao, Z. Natkaniec, A. Natochii, L. Nayak, M. Niiyama, N. K. Nisar, S. Nishida, S. Ogawa, H. Ono, Y. Onuki, P. Oskin, G. Pakhlova, S. Pardi, H. Park, S. Patra, S. Paul, T. K. Pedlar, R. Pestotnik, L. E. Piilonen, E. Prencipe, M. T. Prim, N. Rout, G. Russo, D. Sahoo, S. Sandilya, A. Sangal, L. Santelj, V. Savinov, G. Schnell, C. Schwanda, Y. Seino, K. Senyo, M. E. Sevior, W. Shan, M. Shapkin, C. Sharma, J.-G. Shiu, A. Sokolov, E. Solovieva, M. Starič, M. Sumihama, K. Sumisawa, T. Sumiyoshi, W. Sutcliffe, M. Takizawa, U. Tamponi, K. Tanida, F. Tenchini, M. Uchida, T. Uglov, Y. Unno, S. Uno, S. E. Vahsen, R. van Tonder, G. Varner, A. Vinokurova, E. Waheed, E. Wang, M. Watanabe, S. Watanuki, E. Won, B. D. Yabsley, W. Yan, S. B. Yang, J. Yelton, J. H. Yin, C. Z. Yuan, Z. P. Zhang, and V. Zhilich

(Belle Collaboration)

We report a study of $\Lambda_c^+ \to \Sigma^+\pi^0$, $\Lambda_c^+ \to \Sigma^+\eta$, and $\Lambda_c^+ \to \Sigma^+\eta'$ using the data sample corresponding to an integrated luminosity of 980 fb^{-1} collected with the Belle detector at the KEKB asymmetric-energy e^+e^- collider. The branching fractions relative to $\Lambda_c^+ \to \Sigma^+\pi^0$ are measured as $\mathcal{B}_{\Lambda_c^+ \to \Sigma^+\eta}/\mathcal{B}_{\Lambda_c^+ \to \Sigma^+\pi^0} = 0.25 \pm 0.03 \pm 0.01$ and $\mathcal{B}_{\Lambda_c^+ \to \Sigma^+\eta'}/\mathcal{B}_{\Lambda_c^+ \to \Sigma^+\pi^0} = 0.33 \pm 0.06 \pm 0.02$. Using $\mathcal{B}_{\Lambda_c^+ \to \Sigma^+\pi^0} = (1.25 \pm 0.10)\%$, we obtain $\mathcal{B}_{\Lambda_c^+ \to \Sigma^+\eta} = (3.14 \pm 0.35 \pm 0.17 \pm 0.25) \times 10^{-3}$ and $\mathcal{B}_{\Lambda_c^+ \to \Sigma^+\eta'} = (4.16 \pm 0.75 \pm 0.25 \pm 0.33) \times 10^{-3}$. Here the uncertainties are statistical, systematic, and from $\mathcal{B}_{\Lambda_c^+ \to \Sigma^+\pi^0}$, respectively. The ratio of the branching fraction of $\Lambda_c^+ \to \Sigma^+\eta'$ with respect to that of $\Lambda_c^+ \to \Sigma^+\eta$ is measured to be $\mathcal{B}_{\Lambda_c^+ \to \Sigma^+\eta'}/\mathcal{B}_{\Lambda_c^+ \to \Sigma^+\eta} = 1.34 \pm 0.28 \pm 0.08$. We update the asymmetry parameter of $\Lambda_c^+ \to \Sigma^+\pi^0$, $\alpha_{\Sigma^+\pi^0} = -0.48 \pm 0.02 \pm 0.02$, with a considerably improved precision. The asymmetry parameters of $\Lambda_c^+ \to \Sigma^+\eta$ and $\Lambda_c^+ \to \Sigma^+\eta'$ are measured to be $\alpha_{\Sigma^+\eta} = -0.99 \pm 0.03 \pm 0.05$ and $\alpha_{\Sigma^+\eta'} = -0.46 \pm 0.06 \pm 0.03$ for the first time.

I. INTRODUCTION

Hadronic weak decays of charmed baryons play an important role in understanding the decay dynamics of charmed baryons. For weak decays $\mathbf{B}_c \to \mathbf{B} + \mathbf{M}$, the decay mechanisms involved are W emission and W exchange, where $\mathbf{B}_c$, $\mathbf{B}$, and $\mathbf{M}$ represent the charmed baryon, baryon, and pseudoscalar or vector meson, respectively. The topological diagrams are shown in Fig. 1. Among them, external W emission [Fig. 1(a)] and internal W emission [Fig. 1(b)] are factorizable, while inner W emission [Fig. 1(c)] and W exchange [Figs. 1(d), 1(e), 1(f)] give nonfactorizable contributions. For Cabibbo-allowed two-body decays $\Lambda_c^+ \to \Sigma^+\eta$ and
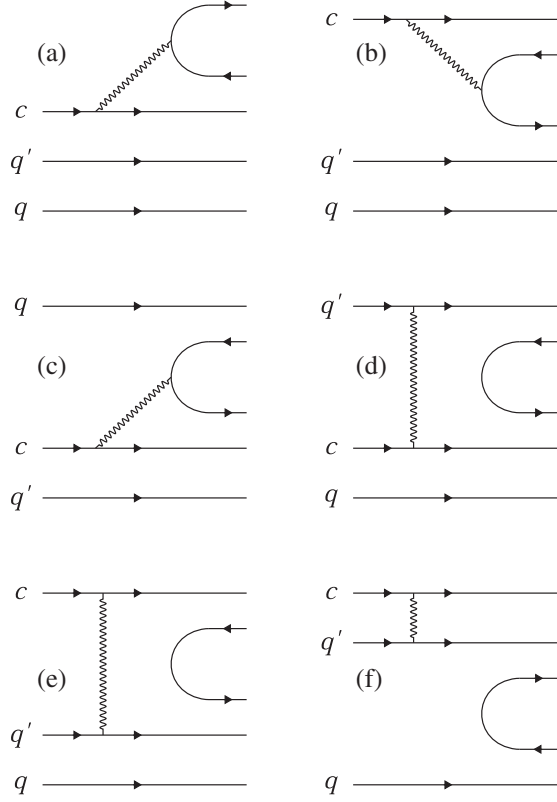
FIG. 1. Topological diagrams contributing to $\mathbf{B}_c \to \mathbf{B} + \mathbf{M}$ decays: (a) external W emission, (b) internal W emission, (c) inner W emission, and (d),(e),(f) W exchange diagrams.

$\Lambda_c^+ \to \Sigma^+ \eta'$, all the nonfactorizable diagrams contribute to these two decays.

To describe the nonfactorizable effects in hadronic decays of charmed baryons, various approaches have been developed, including the covariant confined quark model [1,2], the pole model [3–8], current algebra [9,10] and the SU(3) flavor symmetry [11]. Theoretical calculations on branching fractions of the above two signal decays based on various approaches are listed in Table I. The two branching fractions were measured to be $\mathcal{B}_{\Lambda_c^+ \to \Sigma^+ \eta} = (0.44 \pm 0.20)\%$ and $\mathcal{B}_{\Lambda_c^+ \to \Sigma^+ \eta'} = (1.5 \pm 0.6)\%$, with poor precision [12]. Their ratio is $\mathcal{B}_{\Lambda_c^+ \to \Sigma^+ \eta'}/\mathcal{B}_{\Lambda_c^+ \to \Sigma^+ \eta} = 3.5 \pm 2.1 \pm 0.4$ [13].

The decay asymmetry parameter α was introduced by Lee and Yang to study the parity-violating and parity-conserving amplitudes in weak hyperon decays [15].

Charge conjugation and parity (CP) symmetry implies that the baryon decay asymmetry parameter α equals that of the antibaryon $\bar{\alpha}$ but with an opposite sign [16]. Measuring the asymmetry parameter reveals the degree of parity violation in baryon decays and enables tests of CP symmetry used to search for physics beyond the standard model.

The weak decay asymmetry parameter $\alpha_{\Sigma^+ h^0}$ of the $\Lambda_c^+ \to \Sigma^+ h^0$, $\Sigma^+ \to p\pi^0$ ($h^0 = \pi^0$, η, or η') decays determines the differential decay rate [17],

$$\frac{dN}{d\cos\theta_{\Sigma^+}} \propto 1 + \alpha_{\Sigma^+ h^0}\alpha_{p\pi^0}\cos\theta_{\Sigma^+}, \qquad (1)$$

where θ_{Σ^+} is the angle between the proton momentum vector and the opposite of the Λ_c^+ momentum vector in the Σ^+ rest frame [18] and $\alpha_{p\pi^0} = -0.983 \pm 0.013$ is the averaged asymmetry parameter of $\Sigma^+ \to p\pi^0$ and its charge-conjugated mode [14]. It is related to the parity-violating amplitude A_1 and parity-conserving amplitude A_2 in the decay through [17]

$$\alpha_j = 2\frac{\kappa \text{Re}(A_1 A_2^*)}{|A_1|^2 + \kappa^2 |A_2|^2}, \qquad (2)$$

where $\kappa = pc/(E + mc^2)$ with p, E, and m being the momentum, energy, and mass of the daughter baryon in the rest frame of the parent particle and c is the speed of light, and j denotes the particular decay mode. The asymmetry parameter of $\Lambda_c^+ \to \Sigma^+ \pi^0$ has been measured to be -0.55 ± 0.11, with an uncertainty of about 20% [14]. Up to now, little experimental information on measurements of asymmetry parameters of $\Lambda_c^+ \to \Sigma^+ \eta$ and $\Lambda_c^+ \to \Sigma^+ \eta'$ is available. Theoretical predictions on the asymmetry parameters are calculated based on various models [1,2,7,8,10,11], as listed in Table I.

The isospin symmetry demands that the branching fractions and the asymmetry parameters of $\Lambda_c^+ \to \Sigma^+ \pi^0$ and $\Lambda_c^+ \to \Sigma^0 \pi^+$ shall be equal [11]. Any significant discrepancy would be an indication of isospin breaking, which could be caused by the mass difference between up and down quarks, the electromagnetic interaction, or new physics. Precise measurements of the branching fractions and asymmetry parameters of $\Lambda_c^+ \to \Sigma^+ \pi^0$ and $\Lambda_c^+ \to \Sigma^0 \pi^+$ will provide an excellent test of the isospin symmetry.

In this study, we measure the branching fractions of $\Lambda_c^+ \to \Sigma^+ \eta$ and $\Lambda_c^+ \to \Sigma^+ \eta'$ relative to the $\Lambda_c^+ \to \Sigma^+ \pi^0$

TABLE I. Branching fractions (upper entry) in % and asymmetry parameters (lower entry) in various approaches and in experiment.

Decay	Körner [1]	Ivanov [2]	Żenczykowski [7]	Sharma [8]	Zou [10]	Geng [11]	Experiment [14]
$\Lambda_c^+ \to \Sigma^+ \eta$	0.16	0.11	0.90	0.57	0.74	0.32 ± 0.13	0.44 ± 0.20
$\Lambda_c^+ \to \Sigma^+ \eta'$	1.28	0.12	0.11	0.10	$\cdots$	1.44 ± 056	1.5 ± 0.6
$\Lambda_c^+ \to \Sigma^+ \pi^0$	0.70	0.43	0.39	-0.31	-0.76	-0.35 ± 0.27	$-0.55 + 0.11$
$\Lambda_c^+ \to \Sigma^+ \eta$	0.33	0.35	0.00	-0.91	-0.95	-0.40 ± 0.47	$\cdots$
$\Lambda_c^+ \to \Sigma^+ \eta'$	-0.45	-0.05	-0.91	0.78	0.68	$1.00^{+0.00}_{-0.17}$	$\cdots$

based on the full Belle data. We update the measurement of the asymmetry parameter of $\Lambda_c^+ \to \Sigma^+ \pi^0$ with higher statistics, and measure the asymmetry parameters of $\Lambda_c^+ \to \Sigma^+ \eta$ and $\Lambda_c^+ \to \Sigma^+ \eta'$ for the first time.

II. THE DATA SAMPLE AND THE BELLE DETECTOR

This analysis is based on a data sample corresponding to an integrated luminosity of 980 fb^{-1}, collected with the Belle detector at the KEKB asymmetric-energy $e^+ e^-$ collider [19,20]. About 70% of the data were recorded at the $\Upsilon(4S)$ resonance, and the rest were collected at other $\Upsilon(nS)$ ($n = 1$, 2, 3, or 5) states or at center-of-mass (c.m.) energies a few tens of MeV below the $\Upsilon(4S)$ or the $\Upsilon(nS)$ peaks.

The Belle detector is a large-solid-angle magnetic spectrometer that consists of a silicon vertex detector (SVD), a 50-layer central drift chamber (CDC), an array of aerogel threshold Cherenkov counters (ACC), a barrel-like arrangement of time-of-flight scintillation counters (TOF), and an electromagnetic calorimeter comprised of CsI(Tl) crystals (ECL) located inside a superconducting solenoid coil that provides a 1.5 T magnetic field. An iron flux-return located outside of the coil is instrumented to detect K_L^0 mesons and to identify muons. The detector is described in detail elsewhere [21,22]. The position of the nominal interaction point, where electrons and positrons collide, is defined as the origin of the coordinate system, and the axis aligning with the direction opposite the e^+ beam is defined as the z axis. The ECL is divided into three regions spanning θ, the angle of inclination in the laboratory frame with respect to the z axis, with the backward end cap, barrel and forward end cap regions covering the ranges of $-0.91 < \cos\theta < -0.63$, $-0.63 < \cos\theta < 0.85$, and $0.85 < \cos\theta < 0.98$, respectively.

Monte Carlo (MC) simulated events are used to optimize the selection criteria, study background contributions, and determine the signal reconstruction efficiency. Samples of simulated signal MC events are generated by EVTGEN [23] and propagated through a detector simulation based on GEANT3 [24]. The $e^+ e^- \to c\bar{c}$ events are simulated using PYTHIA [25]; the decays $\eta' \to \eta\pi^+\pi^-$ and $\pi^0/\eta \to \gamma\gamma$ are generated with a phase space model; the decays $\Lambda_c^+ \to \Sigma^+ h^0$ and $\Sigma^+ \to p\pi^0$ are first generated with a phase space model, afterwards corrected using the measured asymmetry parameter to ensure a correct angular distribution. We take into account the effect of final-state radiation from charged particles by using the PHOTOS package [26]. Simulated samples of $\Upsilon(4S) \to B^+B^-/B^0\bar{B}^0$, $\Upsilon(5S) \to B_s^{(*)}\bar{B}_s^{(*)}/B^{(*)}\bar{B}^{(*)}(\pi)/\Upsilon(4S)\gamma$, $e^+ e^- \to q\bar{q}$ ($q = u$, d, s, c) at $\sqrt{s} = 10.52$, 10.58, and 10.867 GeV, and $\Upsilon(1S, 2S, 3S)$ decays, corresponding to 4 times the integrated luminosity of each dataset and normalized to the same integrated luminosity as data, are used to develop the selection criteria

and perform the background study. Charge-conjugate modes are implied throughout this paper unless otherwise stated.

III. EVENT SELECTION

We reconstruct the decays $\Lambda_c^+ \to \Sigma^+ \pi^0$, $\Sigma^+ \eta$, and $\Sigma^+ \eta'$, with $\Sigma^+ \to p\pi^0$, $\eta' \to \eta\pi^+\pi^-$, and $\pi^0/\eta \to \gamma\gamma$.

A set of event selection criteria is chosen to enhance the Λ_c^+ signal while reducing combinatorial background events. These criteria are determined by maximizing the figure of merit $\epsilon/(\frac{5}{2} + \sqrt{n_B})$ [27] for each variable under consideration in an iterative fashion, where ϵ is the signal efficiency; n_B is the number of background events expected in the Λ_c^+ signal region ($\pm 2.5\sigma$ from Λ_c^+ nominal mass [14]).

Charged tracks are identified as proton or pion candidates using information from the tracking (SVD, CDC) and charged-hadron identification (ACC, TOF, CDC) systems combined into a likelihood, $\mathcal{L}(h{:}h') = \mathcal{L}(h)/(\mathcal{L}(h) + \mathcal{L}(h'))$ where h and h' are π, K, or p as appropriate [28]. Tracks having $\mathcal{L}(p{:}\pi) > 0.9$ and $\mathcal{L}(p{:}K) > 0.9$ are identified as proton candidates and having $\mathcal{L}(\pi{:}p) > 0.4$ and $\mathcal{L}(\pi{:}K) > 0.4$ are identified as pion candidates. A likelihood ratio for electron identification, $\mathcal{R}(e)$ formed from ACC, CDC, and ECL information [29], is required to be less than 0.9 for all charged tracks to suppress electrons. The identification efficiencies of p and π are 80% and 95%, respectively. The probabilities of misidentifying h as h', $P(h \to h')$, are estimated to be 2% for $P(p \to \pi)$, 6% for $P(K \to \pi)$, 1% for $P(K \to p)$, and 0.4% for $P(\pi \to p)$. For each charged track, the number of SVD hits in both the z direction and the transverse x–y plane is required at least one. For pion candidates, we require the distance of the closest approach with respect to the interaction point (IP) along the z axis and in the x–y plane to be less than 2.0 and 0.1 cm, respectively.

Photon candidates are selected from ECL clusters not matched to a CDC track trajectory. To reject neutral hadrons, the ratio of the energy deposited in the central 3×3 array of ECL crystals to the total energy deposited in the enclosing 5×5 array of crystals is required to be at least 0.8 for each photon candidate.

The π^0 candidates are reconstructed by combining two photons with an invariant-mass $M(\gamma\gamma)$ between 0.124 and 0.145 GeV/c^2 (around $\pm 2.5\sigma$ of the nominal π^0 mass [14]). We perform a mass-constrained fit to each π^0 candidate to improve the momentum resolution. The daughter photons of π^0 originating from Σ^+ decay are required to have an energy greater than 50 MeV, while for those from Λ_c^+ decay, the energies in the barrel and end caps are required to exceed 50 and 150 MeV, respectively. The reconstructed π^0 momentum in the c.m. frame must exceed 0.1 and 0.8 GeV/c for candidates from Σ^+ and Λ_c^+ decays, respectively.

The η candidates are reconstructed by combining two photons with an invariant-mass $M(\gamma\gamma)$ between 0.523 and 0.567 GeV/c^2 (around $\pm 2.5\sigma$ of the nominal η mass [14]).

To improve the momentum resolution, a mass-constrained fit is performed for η candidates. We require the energy of daughter photons of η originating from $\eta' \to \eta \pi^+ \pi^-$ and $\Lambda_c^+ \to \Sigma^+ \eta$ decays to be greater than 210 and 260 MeV, respectively. The reconstructed η momentum in the c.m. frame is required to be greater than 0.8 GeV/c for $\Lambda_c^+ \to \Sigma^+ \eta$ decay. To further suppress background photons from π^0 decay, we exclude any photon that, in combination with another photon in the event, has a probability of the reconstructed particle to be π^0-like greater than 0.6. The probability is calculated using the invariant mass of the photon pair, the energy of the photon in the laboratory frame, and the angle with respect to the beam direction in the laboratory frame [30].

The η' candidates are reconstructed by combining two oppositely charged π candidates with an η candidate. The candidates with an invariant-mass $M(\eta \pi^+ \pi^-)$ within $(0.953, 0.964)$ GeV/c^2 are retained (around $\pm 2.5\sigma$ of nominal η' mass [14]).

The Σ^+ candidates are formed by combining a π^0 candidate with a proton, with $M(p\pi^0)$ lying between 1.179 and 1.197 GeV/c^2 (around $\pm 2.5\sigma$ of nominal Σ^+ mass [14]). The $\Sigma^+ \to p\pi^0$ reconstruction relies on the long lifetime of the hyperon. We require the proton candidates to have a large (> 1 mm) distance of closest

approach to the IP. The Σ^+ trajectory is approximated by a straight line from the IP in the direction of the reconstructed Σ^+ three-momentum and intersected with the proton path. This point is taken as an estimate of the Σ^+ decay vertex and the π^0 is refit assuming that the $\gamma\gamma$ pair originates from this vertex rather than from the IP. Only Σ^+ candidates with a positive flight length from the IP to the decay vertex are retained. We require a minimum Σ^+ momentum of 1.2 GeV/c in the c.m. frame.

The Λ_c^+ candidates are reconstructed by combining a Σ^+ candidate with a π^0, η, or η' candidate. To suppress background especially from B-meson decays, we require the scaled momentum $x_p > 0.5$, defined as $x_p = p^*/p_{\max}$, where p^* is the three-momentum of Λ_c^+ in the c.m. frame; and $p_{\max} = \sqrt{(E_{\mathrm{beam}}/c)^2 - (Mc)^2}$ is its maximum momentum calculated by the beam energy (E_{beam}) in the c.m. frame and the invariant mass (M) of $\Sigma^+ h^0$ candidates. With the requirement on x_p, the background level can be suppressed by around 90% based on the study of inclusive MC samples. After applying all selections, the fractions of the number of events having more than one Λ_c^+ candidate to those surviving the selections for $\Sigma^+ \pi^0$, $\Sigma^+ \eta$, and $\Sigma^+ \eta'$ modes are 0.8%, 2.2%, and 5.3%, respectively. All the Λ_c^+
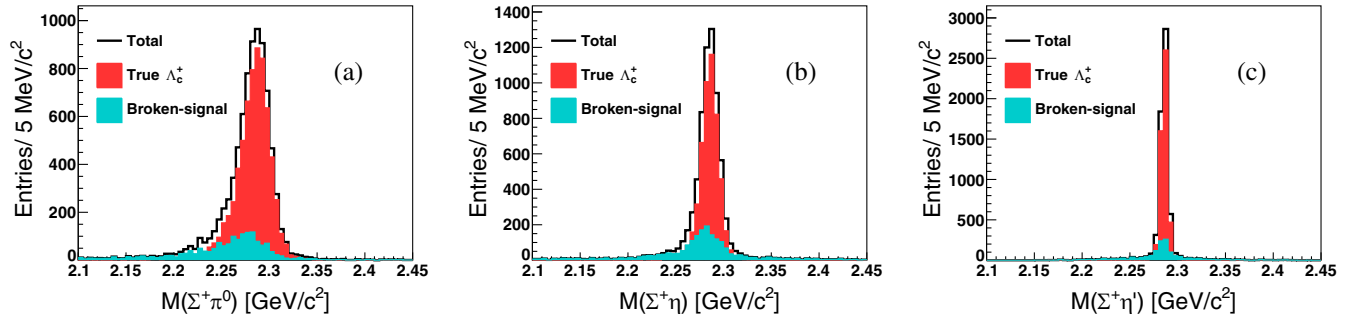

FIG. 2. Distributions of Λ_c^+ invariant mass from signal MC simulation for (a) $\Lambda_c^+ \to \Sigma^+ \pi^0$, (b) $\Lambda_c^+ \to \Sigma^+ \eta$, and (c) $\Lambda_c^+ \to \Sigma^+ \eta'$ modes. The red histogram shows the true Λ_c^+ shape after applying MC-truth matching and the dark cyan histogram shows the shape of broken-signal contribution.
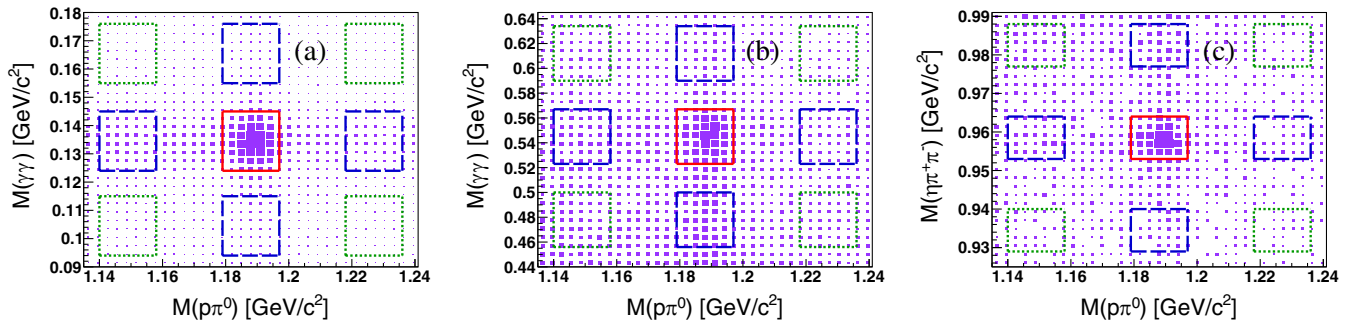

FIG. 3. Two-dimensional distributions of $M(p\pi^0)$ versus $M(\gamma\gamma)$ for (a) $\Lambda_c^+ \to \Sigma^+ \pi^0$ and (b) $\Lambda_c^+ \to \Sigma^+ \eta$, and of $M(p\pi^0)$ versus $M(\eta\pi^+\pi^-)$ for (c) $\Lambda_c^+ \to \Sigma^+ \eta'$ from data. The red box is selected as the Λ_c^+ signal region and the blue and green boxes are selected as sidebands.
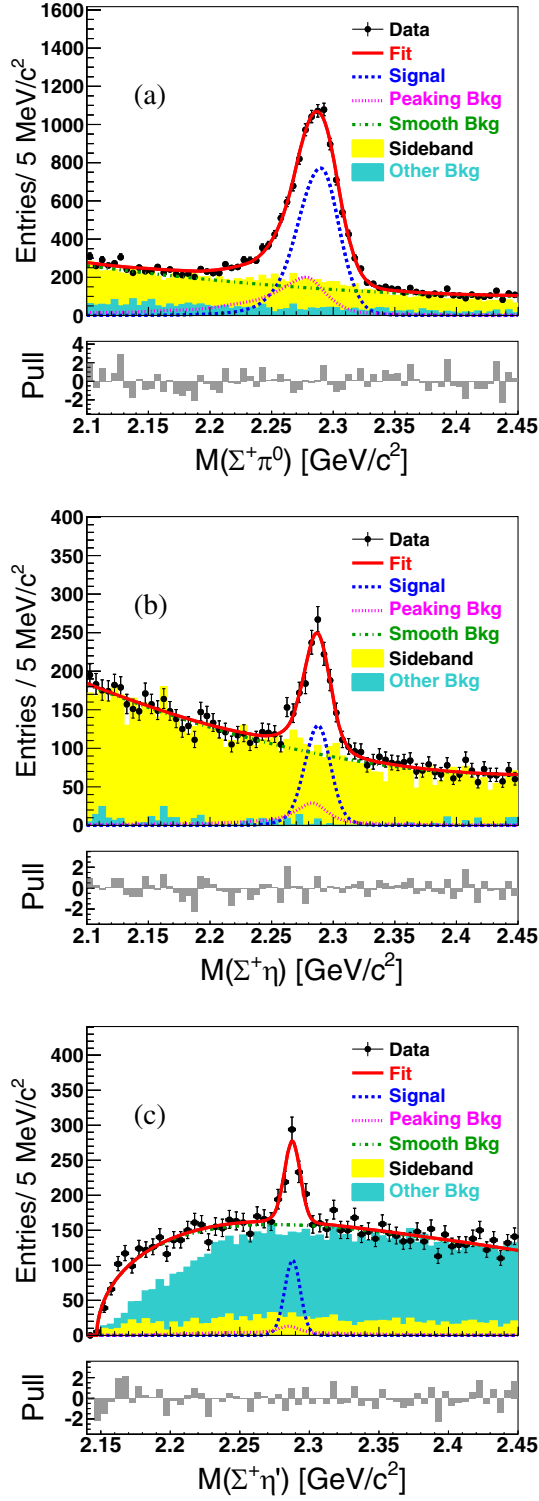
FIG. 4. Invariant mass distributions of (a) $\Sigma^+\pi^0$, (b) $\Sigma^+\eta$, and (c) $\Sigma^+\eta'$ from data. The black dots with error bars represent the data. The red solid line, blue dashed line, magenta dotted line, and dark green dash-dotted line stand for the best fit, signal shape, broken-signal shape, and the background shape, respectively. The yellow histogram is from the normalized sidebands and the dark cyan histogram is from the normalized inclusive MC samples after subtracting the signal process, broken-signal process, and sidebands.

candidates in the mass region of $(2.10, 2.45)$ GeV/c^2 are retained for further analysis.

IV. BACKGROUND STUDY

Using simulations, we search for possible background components that might peak in the Λ_c^+ mass region. A peaking background denoted as the broken-signal contribution, mainly caused by the wrong combination of a real photon with a fake photon to form a π^0 candidate from the Σ^+ decay, is observed in signal MC simulation. The distributions of the true Λ_c^+ events and the broken-signal events for the three modes are shown in Fig. 2, where the red histogram shows the true Λ_c^+ shape and the dark cyan histogram shows the shape of broken-signal contribution. The resolution of the broken-signal is obviously wider than that of the true signal, implying we can separate it from the true signal. The shape of the broken-signal contribution is extracted from MC simulation directly and is treated as a separate background component in the final Λ_c^+ signal yield extraction. The $M(\Sigma^+h^0)$ distributions of the MC sample and data in two-dimensional sidebands described below are consistent, suggesting that the MC simulation is reliable for this broken-signal contribution.

The two-dimensional distributions of $M(p\pi^0)$ versus $M(\gamma\gamma)$ for $\Sigma^+\pi^0$ and $\Sigma^+\eta$ modes, and of $M(p\pi^0)$ versus $M(\eta\pi^+\pi^-)$ for $\Sigma^+\eta'$ mode from data are shown in Fig. 3. The red box is selected as the Λ_c^+ signal region and the blue and green boxes are selected as sidebands. The number of the normalized sideband events is calculated to be 50% of the number of events in blue boxes minus 25% of the number of events in green boxes. The Λ_c^+ mass spectra from the normalized sideband events are shown as the yellow histograms in Fig. 4. The broken-signal also contributes in sidebands and no other peaking components are found. The other background contributions from the inclusive MC samples after subtracting the signal processes, broken-signal processes, and the sidebands are shown in Fig. 4 with dark cyan histograms. The processes of $e^+e^- \rightarrow \Sigma^+h^0 +$ anything could contribute a smooth distribution in the $M(\Sigma^+h^0)$ spectrum, especially for the $\Sigma^+\eta'$ mode. The sum of sidebands in data and other backgrounds in inclusive MC samples can describe the backgrounds in the Λ_c^+ signal region well, indicating that there are no other peaking components. It is verified by the analysis of the inclusive MC samples with TopoAna [31].

V. BRANCHING FRACTION

After applying all the event selections, the invariant mass distributions of $\Sigma^+\pi^0$, $\Sigma^+\eta$, and $\Sigma^+\eta'$ from data are shown in Fig. 4. The Λ_c^+ signal yields are extracted by performing an unbinned maximum-likelihood fit to these invariant-mass spectra. The likelihood function is defined in terms of the signal probability density function (PDF) F_S, broken-signal PDF F_{B1}, and smooth background PDF F_{B2} as

$$\mathcal{L} = \frac{e^{-(n_S+n_{B1}+n_{B2})}}{N!} \prod_i^N [n_S F_S + n_{B1} F_{B1} + n_{B2} F_{B2}], \quad (3)$$

where N is the total number of observed events; n_S, n_{B1}, and n_{B2} are the numbers of Λ_c^+ signal events, broken-signal events, and smooth background events, respectively; i denotes the event index. The numbers of n_S and n_{B2} are floated in the fit. Since the shapes of broken-signal events from the signal region and sidebands agree, we let the number of broken-signal events free in the fit. The F_S PDF is modeled with a histogram from the MC simulated events containing the true Λ_c^+ signal using rookeyspdf [32] and convolved with a Gaussian function, of which the mean and resolution are floated. The Gaussian describes the detector resolution difference between data and MC simulation. The F_{B1} PDF is smoothed with rookeyspdf from the MC simulation to describe the shape of the broken-signal contribution. The F_{B2} PDF is parametrized by a first-order polynomial for the $\Sigma^+\pi^0$ mode, a second-order polynomial for the $\Sigma^+\eta$ mode, and a threshold function for the $\Sigma^+\eta'$ mode. We define the threshold function as $(M - m_0)^\alpha \exp(-\beta(M - m_0))$, where M is the invariant mass of $\Sigma^+\eta'$ and the parameter m_0 is the sum of the nominal masses of Σ^+ and η' [14]. We let the parameters α and β float and m_0 be fixed in the fit. The best fit results for the three modes are shown in Fig. 4, along with the pulls $(N_{\text{data}} - N_{\text{fit}})/\sigma_{\text{data}}$, where σ_{data} is the error on N_{data}.

An ensemble test comprising 1000 pseudoexperiments, where the PDF shapes from fit to data are used, is performed to check for any bias in the fit. We obtain a Gaussian normalized pull distribution width and mean consistent with one and zero within statistical uncertainties, respectively, indicating no fit bias.

The Λ_c^+ signal yields and the signal efficiencies estimated from the signal MC simulations for three modes are summarized in Table II.

The ratios of branching fractions are obtained via

$$\frac{\mathcal{B}_{\Lambda_c^+\to\Sigma^+\eta}}{\mathcal{B}_{\Lambda_c^+\to\Sigma^+\pi^0}} = \frac{(N_{\Sigma^+\eta}/\epsilon_{\Sigma^+\eta})}{(N_{\Sigma^+\pi^0}/\epsilon_{\Sigma^+\pi^0})} \frac{\mathcal{B}_{\pi^0\to\gamma\gamma}}{\mathcal{B}_{\eta\to\gamma\gamma}}, \quad (4)$$

$$\frac{\mathcal{B}_{\Lambda_c^+\to\Sigma^+\eta'}}{\mathcal{B}_{\Lambda_c^+\to\Sigma^+\pi^0}} = \frac{(N_{\Sigma^+\eta'}/\epsilon_{\Sigma^+\eta'})}{(N_{\Sigma^+\pi^0}/\epsilon_{\Sigma^+\pi^0})} \frac{\mathcal{B}_{\pi^0\to\gamma\gamma}}{\mathcal{B}_{\eta'\to\eta\pi^+\pi^-}\mathcal{B}_{\eta\to\gamma\gamma}}, \quad (5)$$

$$\frac{\mathcal{B}_{\Lambda_c^+\to\Sigma^+\eta'}}{\mathcal{B}_{\Lambda_c^+\to\Sigma^+\eta}} = \frac{(N_{\Sigma^+\eta'}/\epsilon_{\Sigma^+\eta'})}{(N_{\Sigma^+\eta}/\epsilon_{\Sigma^+\eta})} \frac{1}{\mathcal{B}_{\eta'\to\eta\pi^+\pi^-}}, \quad (6)$$

where $N_{\Sigma^+\eta}$, $N_{\Sigma^+\eta'}$, and $N_{\Sigma^+\pi^0}$ are the Λ_c^+ signal yields for the three modes; $\epsilon_{\Sigma^+\eta}$, $\epsilon_{\Sigma^+\eta'}$, and $\epsilon_{\Sigma^+\pi^0}$ are the signal

efficiencies; $\mathcal{B}_{\pi^0/\eta\to\gamma\gamma}$ and $\mathcal{B}_{\eta'\to\eta\pi^+\pi^-}$ are the branching fractions of decays of the intermediate states. We obtain

$$\frac{\mathcal{B}_{\Lambda_c^+\to\Sigma^+\eta}}{\mathcal{B}_{\Lambda_c^+\to\Sigma^+\pi^0}} = 0.25 \pm 0.03 \pm 0.01, \quad (7)$$

$$\frac{\mathcal{B}_{\Lambda_c^+\to\Sigma^+\eta'}}{\mathcal{B}_{\Lambda_c^+\to\Sigma^+\pi^0}} = 0.33 \pm 0.06 \pm 0.02, \quad (8)$$

$$\frac{\mathcal{B}_{\Lambda_c^+\to\Sigma^+\eta'}}{\mathcal{B}_{\Lambda_c^+\to\Sigma^+\eta}} = 1.34 \pm 0.28 \pm 0.06, \quad (9)$$

where the first uncertainty is statistical and the second systematic, as discussed in Sec. VII A.

VI. ASYMMETRY PARAMETER

The differential decay rate depends on the asymmetry parameter $\alpha_{\Sigma^+h^0}$ as

$$\frac{dN}{d\cos\theta_{\Sigma^+}} \propto 1 + \alpha_{\Sigma^+h^0}\alpha_{p\pi^0}\cos\theta_{\Sigma^+}. \quad (10)$$

We divide the $\cos\theta_{\Sigma^+}$ distribution into five bins. The Λ_c^+ signal yield in each bin is obtained by fitting the corresponding $M(\Sigma^+h^0)$ distribution with a method similar to that used in the overall fit. The fits to the $M(\Sigma^+h^0)$ distributions in each bin of $\cos\theta_{\Sigma^+}$ are shown in the Appendix. Due to limited statistics, the fraction of n_S to n_{B1} and the values of the mean and resolution of the Gaussian function are fixed to those from overall fits for $\Sigma^+\eta$ and $\Sigma^+\eta'$ modes. No dependence of n_S/n_{B1} on $\cos\theta_{\Sigma^+}$ is found in data for the $\Sigma^+\pi^0$ mode, and none is found in MC simulation for the $\Sigma^+\eta$ and $\Sigma^+\eta'$ modes, so fixing this ratio from MC simulation is reasonable. Table III lists the signal yields and signal efficiencies in the five $\cos\theta_{\Sigma^+}$ bins for the three decays.

The final efficiency-corrected $\cos\theta_{\Sigma^+}$ distributions for $\Lambda_c^+ \to \Sigma^+\pi^0$, $\Lambda_c^+ \to \Sigma^+\eta$, and $\Lambda_c^+ \to \Sigma^+\eta'$ decays are shown in Fig. 5. Using the function $dN/d\cos\theta_{\Sigma^+} \propto 1 + \alpha_{\Sigma^+h^0}\alpha_{p\pi^0}\cos\theta_{\Sigma^+}$ to fit the efficiency-corrected $\cos\theta_{\Sigma^+}$ distributions, where the parameter $\alpha_{\Sigma^+h^0}\alpha_{p\pi^0}$ is floating in the fit, we obtain

$$\alpha_{\Sigma^+\pi^0}\alpha_{p\pi^0} = 0.47 \pm 0.02, \quad (11)$$

TABLE II. The Λ_c^+ signal yields and the signal efficiencies for different decay modes.

Mode	$\Lambda_c^+ \to \Sigma^+\pi^0$	$\Lambda_c^+ \to \Sigma^+\eta$	$\Lambda_c^+ \to \Sigma^+\eta'$
Signal yield	6965 ± 142	719 ± 78	307 ± 55
Efficiency (%)	0.63	0.67	0.50

TABLE III. The values of $\frac{\text{Signal yields}}{\text{Efficiency (\%)}}$ in different $\cos\theta_{\Sigma^+}$ bins for $\Sigma^+\pi^0$, $\Sigma^+\eta$, and $\Sigma^+\eta'$ modes.

$\cos\theta_{\Sigma^+}$	$(-1, -0.6)$	$(-0.6, -0.2)$	$(-0.2, 0.2)$	$(0.2, 0.6)$	$(0.6, 1)$
$\Sigma^+\pi^0$	$\frac{1019\pm98}{0.69}$	$\frac{1240\pm104}{0.67}$	$\frac{1350\pm117}{0.62}$	$\frac{1619\pm129}{0.59}$	$\frac{1967\pm131}{0.61}$
$\Sigma^+\eta$	$\frac{44\pm20}{0.75}$	$\frac{69\pm21}{0.72}$	$\frac{129\pm27}{0.67}$	$\frac{223\pm32}{0.67}$	$\frac{256\pm35}{0.63}$
$\Sigma^+\eta'$	$\frac{46\pm18}{0.51}$	$\frac{47\pm17}{0.51}$	$\frac{62\pm19}{0.49}$	$\frac{54\pm18}{0.50}$	$\frac{102\pm21}{0.49}$

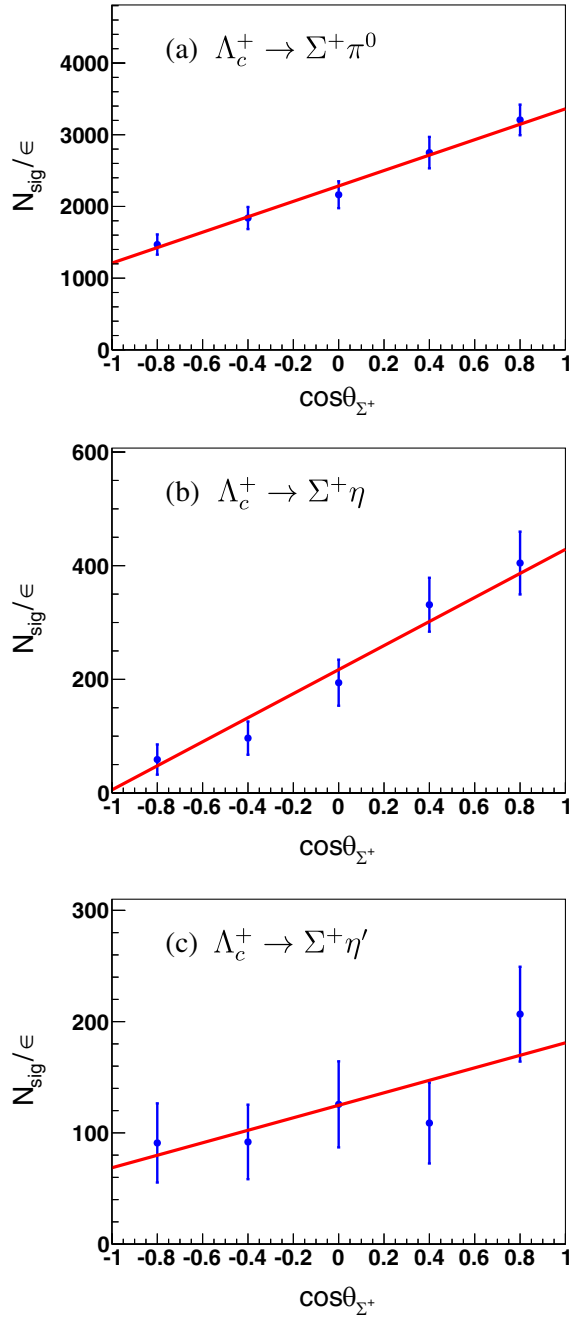FIG. 5. The maximum likelihood fits to the efficiency-corrected $\cos\theta_{\Sigma^+}$ distributions of data to extract (a) $\alpha_{\Sigma^+\pi^0}$, (b) $\alpha_{\Sigma^+\eta}$, and (c) $\alpha_{\Sigma^+\eta'}$. The points with error bars represent data and the red solid lines are the best fits.

$$\alpha_{\Sigma^+\eta}\alpha_{p\pi^0} = 0.97 \pm 0.03, \tag{12}$$

$$\alpha_{\Sigma^+\eta'}\alpha_{p\pi^0} = 0.45 \pm 0.06, \tag{13}$$

where the uncertainties are statistical. Using $\alpha_{p\pi^0} = -0.983 \pm 0.013$ [14], we calculate the asymmetry parameters

$$\alpha_{\Sigma^+\pi^0} = -0.48 \pm 0.02 \pm 0.02, \tag{14}$$

$$\alpha_{\Sigma^+\eta} = -0.99 \pm 0.03 \pm 0.05, \tag{15}$$

$$\alpha_{\Sigma^+\eta'} = -0.46 \pm 0.06 \pm 0.03, \tag{16}$$

where the uncertainties are statistical and systematic, respectively. Section VII B discusses the details of systematic uncertainty.

VII. SYSTEMATIC UNCERTAINTIES

A. Ratio of the branching fractions

Systematic uncertainties in the ratios of branching fractions are summarized in Table IV. The sources include particle identification (PID), charged-track reconstruction, mass windows of intermediate states, fit range, background PDF, signal PDF, broken-signal PDF, the number of broken-signal events, asymmetry parameter, branching fractions of intermediate states, and MC statistics. The systematic uncertainty from $\Sigma^+ \rightarrow p\pi^0$ reconstruction cancels for the three ratios, including the efficiency of proton selection and reconstruction, photon reconstruction, and mass window of Σ^+.

Based on the study of $D^{*+} \rightarrow D^0(\rightarrow K^-\pi^+)\pi^+$, the PID uncertainty is 1.2% for π^+ selection, and 1.3% for π^- selection. We use partially reconstructed D^{*+} decays in $D^{*+} \rightarrow \pi^+ D^0(\rightarrow K_S^0\pi^+\pi^-)$ to assign the systematic uncertainty from charged-track reconstruction (0.35% per track).

The ratios of the efficiencies between data and MC simulations are 0.986 ± 0.004, 1.009 ± 0.008, and 0.989 ± 0.011 for mass windows of π^0, η, and η', respectively. The central values of the ratios are taken as the efficiency correction factors and the uncertainties are taken as systematic uncertainties due to mass windows of the intermediate states.

We perform the simulated pseudoexperiments to estimate the uncertainty from the fit procedure. An ensemble of

TABLE IV. Relative systematic uncertainties (in %) in ratios of branching fractions.

Source	$\dfrac{\mathcal{B}_{\Lambda_c^+\rightarrow\Sigma^+\eta}}{\mathcal{B}_{\Lambda_c^+\rightarrow\Sigma^+\pi^0}}$	$\dfrac{\mathcal{B}_{\Lambda_c^+\rightarrow\Sigma^+\eta'}}{\mathcal{B}_{\Lambda_c^+\rightarrow\Sigma^+\pi^0}}$	$\dfrac{\mathcal{B}_{\Lambda_c^+\rightarrow\Sigma^+\eta'}}{\mathcal{B}_{\Lambda_c^+\rightarrow\Sigma^+\eta}}$
PID	$\cdots$	2.5	2.5
Track reconstruction	$\cdots$	0.7	0.7
Mass window	0.9	1.4	1.1
Fit range	1.9	1.2	1.6
Background PDF	1.4	3.0	2.9
Signal PDF	0.5	0.2	0.7
Broken-signal PDF	1.2	1.1	0.8
Number of broken-signal	4.2	3.6	2.5
Asymmetry parameter	1.7	0.5	1.7
Branching fraction	0.5	1.3	1.2
MC statistics	1.4	1.5	1.5
Total	5.6	6.1	5.7

1000 pseudoexperiments is generated using the mass distributions of Λ_c^+ in Fig. 4 and fitted with a changed likelihood function. The distribution of the fitted Λ_c^+ signal yields is fitted by a Gaussian function and the difference between the mean of Gaussian and the nominal value is taken as the systematic uncertainty. The changes of fit condition include (1) changing the fit range to (2.15, 2.40) GeV/c^2; (2) changing the background PDF from a first-order polynomial to a second-order one for $\Lambda_c^+ \to \Sigma^+ \pi^0$, from a second-order polynomial to a third-order one for $\Lambda_c^+ \to \Sigma^+ \eta$, and from a threshold function to an ARGUS function [33] for $\Lambda_c^+ \to \Sigma^+ \eta'$; (3) using the signal shape smoothed by roohistpdf [34]; (4) using the broken-signal shape smoothed by roohistpdf. We add the uncertainties in quadrature for the corresponding ratios of branching fractions.

The number of broken-signal events is floating in the nominal fit to account for the contribution from broken-signal in sidebands. Considering the possibility of overestimation or underestimation of the broken-signal contribution, we fix the number of broken-signal events according to the MC simulation, and take the difference in ratio of branching fractions as the systematic uncertainty.

The signal MC samples are corrected using the measured asymmetry parameters. We vary the asymmetry parameter by $\pm 1\sigma$ and take the maximum difference on the signal efficiency with respect to the nominal value as the systematic uncertainty, which is 0.4% for the $\Sigma^+ \pi^0$ mode, 1.7% for the $\Sigma^+ \eta$ mode, and 0.3% for the $\Sigma^+ \eta'$ mode. We add them in quadrature for the corresponding ratios of branching fractions.

The systematic uncertainties from $\mathcal{B}_{\pi^0 \to \gamma\gamma}$, $\mathcal{B}_{\eta' \to \eta\pi^+\pi^-}$, and $\mathcal{B}_{\eta \to \gamma\gamma}$ are 0.03%, 1.2%, and 0.5%, respectively [14]. The systematic uncertainty due to MC statistics in the signal efficiency is calculated as $\sqrt{(1-\epsilon)/(\epsilon N_{\mathrm{gen}})}$, where ϵ is the signal efficiency and N_{gen} is the number of generated Λ_c^+ simulated events.

B. Asymmetry parameter

Systematic uncertainties in asymmetry parameters are summarized in Table V. The sources include mass resolution, fit range, background PDF, signal PDF, broken-signal PDF, the number of broken-signal events, the number of $\cos\theta_{\Sigma^+}$ bins, and $\alpha_{p\pi^0}$.

The systematic uncertainties from the fit are estimated using simulated pseudoexperiments. We use an ensemble of pseudoexperiments to generate the mass spectra of Λ_c^+ candidates from data samples. The number of signal events in each $\cos\theta_{\Sigma^+}$ bin is obtained by fitting the generated mass spectra after enlarging the mass resolution by 10%, and changing the fit range, background shape, signal shape, and broken-signal shape. After 1000 simulations, distributions of $\alpha_{\Sigma^+ h^0}$ are obtained by fitting the slopes of the $\cos\theta_{\Sigma^+}$ distributions. The differences between the fitted values of

TABLE V. Relative systematic uncertainties (in %) in asymmetry parameters.

Source	$\alpha_{\Sigma^+\pi^0}$	$\alpha_{\Sigma^+\eta}$	$\alpha_{\Sigma^+\eta'}$
Mass resolution	$\cdots$	1.4	2.9
Fit range	1.6	2.7	2.1
Background shape	1.1	1.9	1.0
Signal PDF	0.3	0.4	0.1
Broken-signal PDF	0.7	1.0	1.2
Number of broken-signal	2.4	$\cdots$	$\cdots$
$\cos\theta_{\Sigma^+}$ bins	1.9	2.8	4.7
$\alpha_{p\pi^0}$	1.3	1.3	1.3
Total	3.9	4.8	6.2

the distributions of $\alpha_{\Sigma^+ h^0}$ with Gaussian functions and the nominal values are taken as the uncertainties. The changed fit range, background shape, signal shape, and broken-signal shape follow those in Sec. VII A. The parameters of the Gaussian describing the resolution difference between data and MC simulation are not fixed in $\alpha_{\Sigma^+ \pi^0}$ extraction, thus no uncertainty from mass resolution is considered.

The number of broken-signal events is floating for $\Sigma^+ \pi^0$ mode and fixed for another two modes. To estimate the uncertainty from the number of broken-signal events, we fix the number based on the MC simulation, and take the difference in asymmetry parameters as the systematic uncertainty.

We change the number of $\cos\theta_{\Sigma^+}$ bins from five to four or to six, and take the maximum difference on the asymmetry parameter as the systematic uncertainty. The systematic uncertainty from $\alpha_{p\pi^0}$ is 1.3% [14].

VIII. SUMMARY

We analyze the $\Sigma^+ h^0$ final states to study Λ_c^+ decays using the full Belle data corresponding to an integrated luminosity of 980 fb^{-1}. The branching fractions of $\Lambda_c^+ \to \Sigma^+ \eta$ and $\Lambda_c^+ \to \Sigma^+ \eta'$ relative to that of the $\Lambda_c^+ \to \Sigma^+ \pi^0$ decay mode are measured to be

$$\frac{\mathcal{B}_{\Lambda_c^+ \to \Sigma^+ \eta}}{\mathcal{B}_{\Lambda_c^+ \to \Sigma^+ \pi^0}} = 0.25 \pm 0.03 \pm 0.01, \tag{17}$$

$$\frac{\mathcal{B}_{\Lambda_c^+ \to \Sigma^+ \eta'}}{\mathcal{B}_{\Lambda_c^+ \to \Sigma^+ \pi^0}} = 0.33 \pm 0.06 \pm 0.02, \tag{18}$$

where the uncertainties, here and below, are statistical and systematic, respectively. Taking $\mathcal{B}_{\Lambda_c^+ \to \Sigma^+ \pi^0} = (1.25 \pm 0.10)\%$ [14], the absolute branching fractions are

$$\mathcal{B}_{\Lambda_c^+ \to \Sigma^+ \eta} = (3.14 \pm 0.35 \pm 0.17 \pm 0.25) \times 10^{-3}, \tag{19}$$

$$\mathcal{B}_{\Lambda_c^+ \to \Sigma^+ \eta'} = (4.16 \pm 0.75 \pm 0.25 \pm 0.33) \times 10^{-3}, \tag{20}$$

where the third uncertainty is from $\mathcal{B}_{\Lambda_c^+ \to \Sigma^+ \pi^0}$. The measured results are the most precise results to date and agree with earlier results [14] within 2 standard deviations.

The ratio of $\mathcal{B}_{\Lambda_c^+ \to \Sigma^+ \eta'}$ to $\mathcal{B}_{\Lambda_c^+ \to \Sigma^+ \eta}$ is determined to be

$$\frac{\mathcal{B}_{\Lambda_c^+ \to \Sigma^+ \eta'}}{\mathcal{B}_{\Lambda_c^+ \to \Sigma^+ \eta}} = 1.34 \pm 0.28 \pm 0.08, \qquad (21)$$

in which the value of the ratio is consistent with one within 1.2 standard deviations.

The asymmetry parameters $\alpha_{\Sigma^+ \eta}$ and $\alpha_{\Sigma^+ \eta'}$ are measured for the first time. The values are

$$\alpha_{\Sigma^+ \eta} = -0.99 \pm 0.03 \pm 0.05, \qquad (22)$$

$$\alpha_{\Sigma^+ \eta'} = -0.46 \pm 0.06 \pm 0.03. \qquad (23)$$

The asymmetry parameter $\alpha_{\Sigma^+ \pi^0}$ is measured as

$$\alpha_{\Sigma^+ \pi^0} = -0.48 \pm 0.02 \pm 0.02, \qquad (24)$$

which agrees with the world average value [14] with the uncertainty considerably improved from 20% to 6%. Comparing the measured result with $\alpha_{\Sigma^0 \pi^+} = -0.463 \pm 0.016 \pm 0.008$ as measured by Belle [35], their agreement within 1 standard deviation shows consistency with the prediction from the isospin symmetry [11].

Comparing with the theoretical predictions summarized in Table I, all the theoretical methods could not predict the $\mathcal{B}_{\Lambda_c^+ \to \Sigma^+ \eta'}$ well and only the result using the method based on the heavy quark effective theory (HQEF) [8] is basically consistent with the measured $\mathcal{B}_{\Lambda_c^+ \to \Sigma^+ \eta}$. Comparing with the theoretical predictions summarized in Table I, we note that none of the methods is able to account for all three measured decay asymmetries. The approaches based on the HQEF [8] and the constituent quark model [10] could successfully predict the $\alpha_{\Sigma^+ \eta}$. The measured $\alpha_{\Sigma^+ \pi^0}$ and $\alpha_{\Sigma^+ \eta'}$ are consistent with the predictions based on $SU(3)_F$ flavor symmetry [11] and spectator quark model [1], respectively. The other approaches failed in predicting the asymmetry parameters of the above three modes.

APPENDIX: $M(\Sigma^+ h^0)$ SPECTRA IN $\cos \theta_{\Sigma^+}$ BINS

The fits to the $M(\Sigma^+ h^0)$ spectra in bins of $\cos \theta_{\Sigma^+}$ are shown in Fig. 6 for $\Sigma^+ \pi^0$ mode, in Fig. 7 for $\Sigma^+ \eta$ mode, and in Fig. 8 for $\Sigma^+ \eta'$ mode.
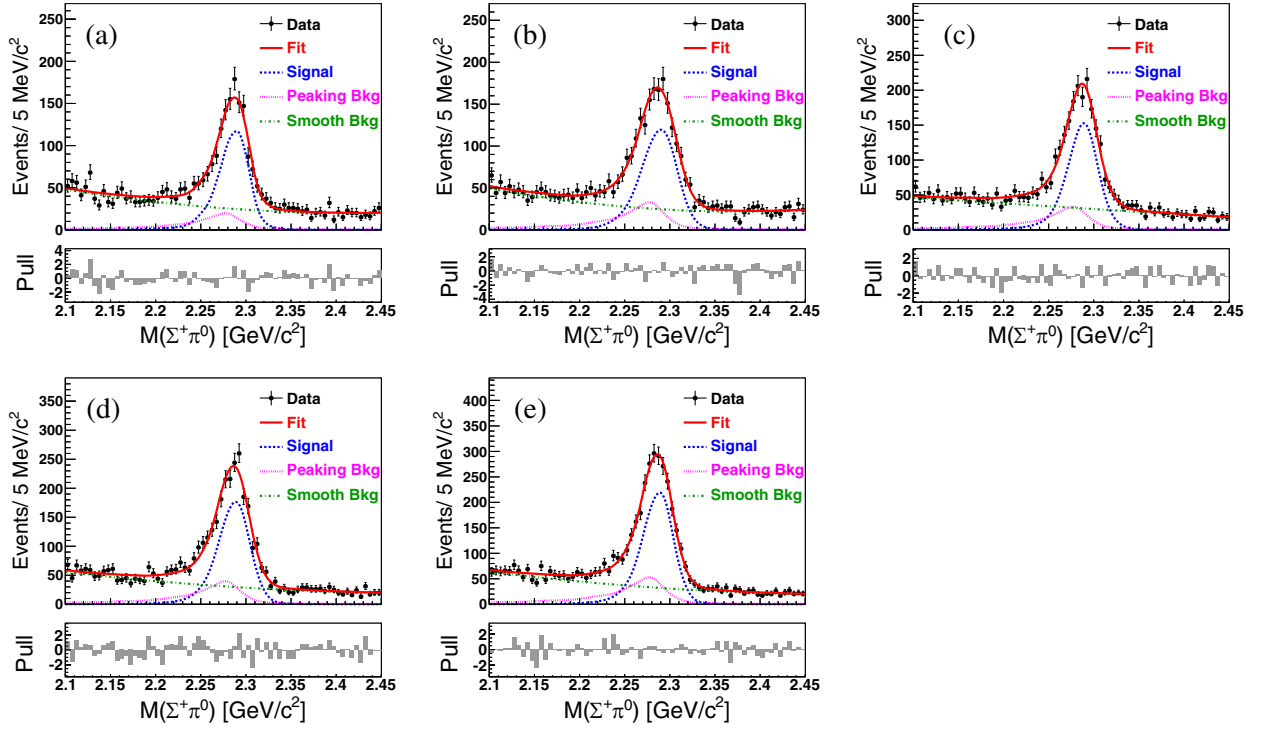
FIG. 6. Fits to $M(\Sigma^+\pi^0)$ distributions from data in (a) $-1.0 < \cos\theta_{\Sigma^+} < -0.6$, (b) $-0.6 < \cos\theta_{\Sigma^+} < -0.2$, (c) $-0.2 < \cos\theta_{\Sigma^+} < 0.2$, (d) $0.2 < \cos\theta_{\Sigma^+} < 0.6$, and (e) $0.6 < \cos\theta_{\Sigma^+} < 1.0$.
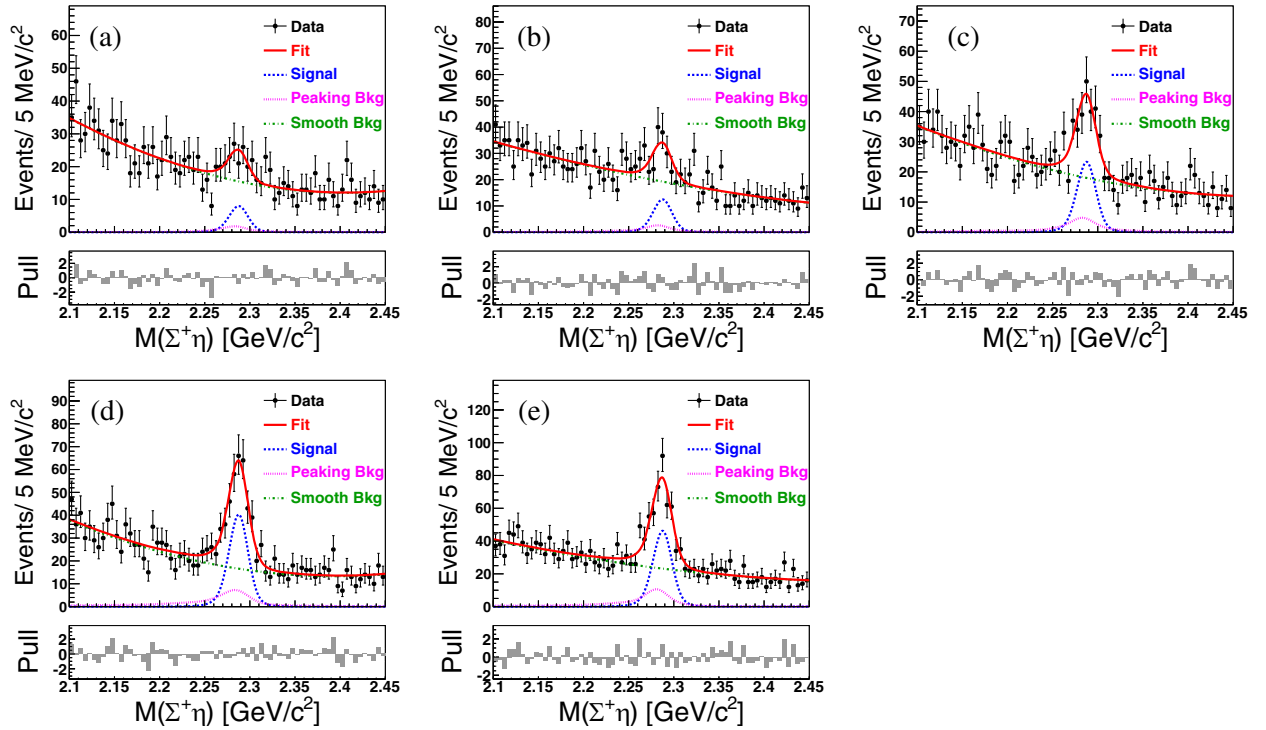

FIG. 7. Fits to $M(\Sigma^+\eta)$ distributions from data in (a) $-1.0 < \cos\theta_{\Sigma^+} < -0.6$, (b) $-0.6 < \cos\theta_{\Sigma^+} < -0.2$, (c) $-0.2 < \cos\theta_{\Sigma^+} < 0.2$, (d) $0.2 < \cos\theta_{\Sigma^+} < 0.6$, and (e) $0.6 < \cos\theta_{\Sigma^+} < 1.0$.
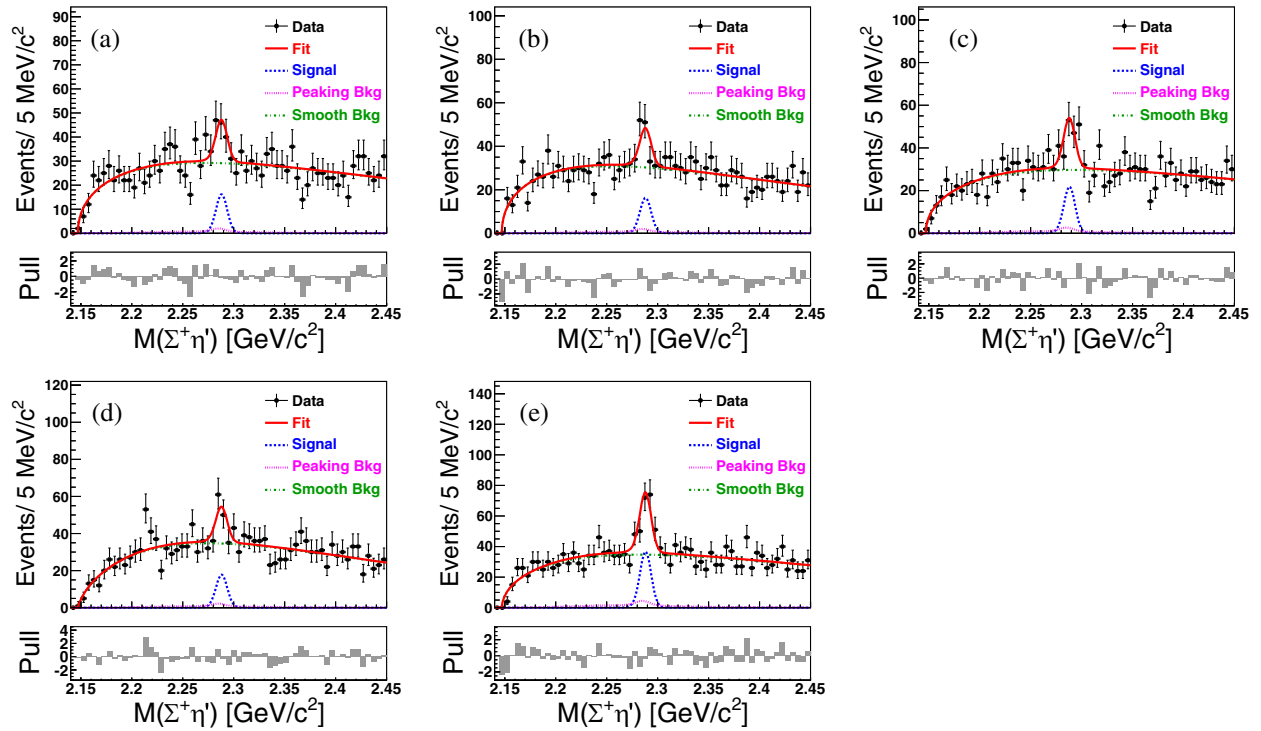
FIG. 8.   Fits to $M(\Sigma^{+}\eta')$ distributions from data in (a) $-1.0 < \cos\theta_{\Sigma^{+}} < -0.6$, (b) $-0.6 < \cos\theta_{\Sigma^{+}} < -0.2$, (c) $-0.2 < \cos\theta_{\Sigma^{+}} < 0.2$, (d) $0.2 < \cos\theta_{\Sigma^{+}} < 0.6$, and (e) $0.6 < \cos\theta_{\Sigma^{+}} < 1.0$.

[1] J. G. Körner and M. Krämer, Z. Phys. C **55**, 659 (1992).

[2] M. A. Ivanov, J. G. Körner, V. E. Lyubovitskij, and A. G. Tusetsky, Phys. Rev. D **57**, 5632 (1998).

[3] H. Y. Cheng and B. Tseng, Phys. Rev. D **46**, 1042 (1992); **55**, 1697 (1997).

[4] Q. P. Xu and A. N. Kamal, Phys. Rev. D **46**, 270 (1992).

[5] H. Y. Cheng and B. Tseng, Phys. Rev. D **48**, 4188 (1993).

[6] Q. P. Xu and A. N. Kamal, Phys. Rev. D **46**, 3836 (1992).

[7] P. Żenczykowski, Phys. Rev. D **50**, 5787 (1994).

[8] K. K. Sharma and R. C. Verma, Eur. Phys. J. C **7**, 217 (1999).

[9] J. G. Körner, G. Kramer, and J. Willrodt, Phys. Lett. **78B**, 492 (1978).

[10] T. Uppal, R. C. Verma, and M. P. Khanna, Phys. Rev. D **49**, 3417 (1994).

[11] C. Q. Geng, C. W. Liu, and T. H. Tsai, Phys. Lett. B **794**, 19 (2019).

[12] M. Ablikim et al. (BESIII Collaboration), Chin. Phys. C **43**, 083002 (2019).

[13] H. Y. Cheng, Chin. J. Phys. **78**, 324 (2022).

[14] R. L. Workman et al. (Particle Data Group), Prog. Theor. Exp. Phys. **2022**, 083C01 (2022).

[15] T. D. Lee and C. N. Yang, Phys. Rev. **108**, 1645 (1957).

[16] M. Ablikim et al. (BESIII Collaboration), Nature (London) **606**, 64 (2022).

[17] R. E. Behrends, Phys. Rev. **111**, 1691 (1958).

[18] P. Bialas, J. G. Körner, M. Krämer, and K. Zalewski, Z. Phys. C **57**, 115 (1993).

[19] S. Kurokawa and E. Kikutani, Nucl. Instrum. Methods Phys. Res., Sect. A **499**, 1 (2003), and other papers included in this volume.

[20] T. Abe et al., Prog. Theor. Exp. Phys. **2013**, 03A001 (2013), and references therein.

[21] J. Brodzicka et al., Prog. Theor. Exp. Phys. **2012**, 04D001 (2012).

[22] A. Abashian et al. (Belle Collaboration), Nucl. Instrum. Methods Phys. Res., Sect. A **479**, 117 (2002).

[23] D. J. Lange, Nucl. Instrum. Methods Phys. Res., Sect. A **462**, 152 (2001).

[24] R. Brun et al., GEANT 3: User's guide Geant 3.10, Geant 3.11, CERN Report No. DD/EE/84-1, 1984.

[25] T. Sjöstrand, S. Mrenna, and P. Skands, Comput. Phys. Commun. **178**, 852 (2008).

[26] E. Barberio and Z. Was, Comput. Phys. Commun. **79**, 291 (1994).

[27] G. Punzi, arXiv:physics/0308063.

[28] E. Nakano, Nucl. Instrum. Methods Phys. Res., Sect. A **494**, 402 (2002).

[29] K. Hanagaki, H. Kakuno, H. Ikeda, T. Iijima, and T. Tsukamoto, Nucl. Instrum. Methods Phys. Res., Sect. A **485**, 490 (2002).

[30] P. Koppenburg *et al.* (Belle Collaboration), Phys. Rev. Lett. **93**, 061803 (2004).

[31] X. Y. Zhou, S. X. Du, G. Li, and C. P. Shen, Comput. Phys. Commun. **258**, 107540 (2021).

[32] K. S. Cranmer, Comput. Phys. Commun. **136**, 198 (2001).

[33] H. Albrecht *et al.* (ARGUS Collaboration), Phys. Lett. B **241**, 278 (1990).

[34] I. Antcheva *et al.*, Comput. Phys. Commun. **180**, 2499 (2009).

[35] L. K. Li *et al.* (Belle Collaboration), arXiv:2208.08695.